

# FaceLift: Single Image to 3D Head with View Generation and GS-LRM

Weijie Lyu<sup>1\*</sup> Yi Zhou<sup>2</sup> Ming-Hsuan Yang<sup>1</sup> Zhixin Shu<sup>2†</sup>

<sup>1</sup>University of California, Merced <sup>2</sup>Adobe Research

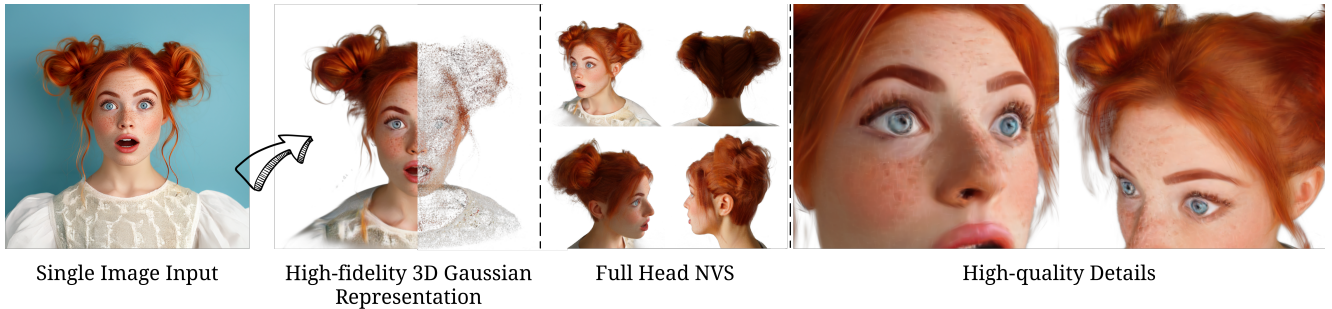


Figure 1. *FaceLift* takes a single image of a human face as input and generates a high-fidelity 3D Gaussian head representation. We present the rendering result on the left side and the centers of the Gaussians on the right side for visualization. The generated Gaussian representation enables high-quality, full-head novel view synthesis (NVS) while accurately capturing fine details of the face and hair.

## Abstract

We present *FaceLift*, a feed-forward approach for rapid, high-quality 360-degree head reconstruction from a single image. Our pipeline begins by employing a multi-view latent diffusion model that generates consistent side and back views of the head from a single facial input. These generated views then serve as input to a GS-LRM reconstructor, which produces a comprehensive 3D representation using Gaussian splats. To train our system, we develop a dataset of multi-view renderings using synthetic 3D human head assets. The diffusion-based multi-view generator is trained exclusively on synthetic head images, while the GS-LRM reconstructor undergoes initial training on Objaverse followed by fine-tuning on synthetic head data. *FaceLift* excels at preserving identity and maintaining view consistency across views. Despite being trained solely on synthetic data, *FaceLift* demonstrates remarkable generalization to real-world images. Through extensive qualitative and quantitative evaluations, we show that *FaceLift* outperforms state-of-the-art methods in 3D head reconstruction, highlighting its practical applicability and robust performance on real-world images. In addition to single image reconstruction, *FaceLift* supports video inputs for 4D novel view synthesis and seamlessly integrates with 2D reanimation techniques to enable 3D facial animation. Project page: <https://weijielyu.github.io/FaceLift>.

\*Work was done when Weijie Lyu was an intern at Adobe Research.

†Corresponding author.

## 1. Introduction

3D head reconstruction has been a central focus in computer vision and computer graphics research for decades, driven by its crucial applications in virtual and augmented reality, digital entertainment, and telepresence systems. The task remains particularly challenging because the human visual system is highly attuned to facial details, making even subtle rendering artifacts far more noticeable than those in other objects.

Traditional approaches to 3D head synthesis typically use parametric textured mesh models [27, 54] trained on large 3D scan datasets. While these models enable basic head generation, the resulting rendered images often lack fine-scale geometric and textural details, which limits their perceptual realism and expressive capabilities. Recent breakthroughs in image generative models [15, 19] and novel view synthesis techniques [23, 35] have opened new possibilities for this research area. Leveraging these developments, recent works [1, 62] use neural 3D representations and large, unstructured face image datasets to learn effective 3D head representations without requiring explicit multi-view consistency in the training data. A parallel approach such as RodinHD [63] leverages synthetic multi-view images to train generative models that directly output 3D neural representations of the head. However, training solely on synthetic data often results in significant perceptual identity loss in the generated outputs, as demonstrated in Fig. 2.

Diffusion-based view generation methods have achieved

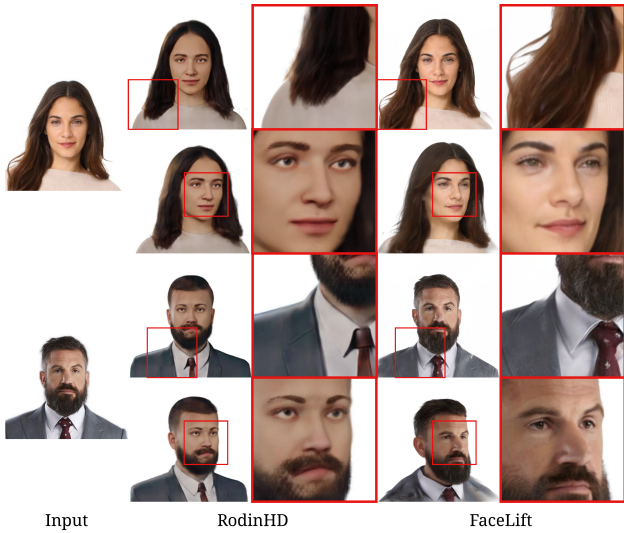


Figure 2. RodinHD [63] trains triplane diffusion with only synthetic data, resulting in apparent identity loss. By leveraging stable diffusion priors [42], *FaceLift* achieves better identity preservation and generalizes effectively to real human portraits.

remarkable results in text-to-3D and image-to-3D tasks [25, 26, 31, 32, 47]. These approaches leverage text-to-image foundation models trained on vast internet data, combined with training on synthetic 3D object renderings [8, 9], demonstrating impressive generalization capabilities for general object view synthesis. However, due to the high perceptual sensitivity of human faces, we show that models trained solely on object data fail to generalize effectively to 3D human face reconstruction.

Inspired by this, we present *FaceLift*, a two-stage pipeline for high-quality 3D head reconstruction from a single image. The first stage builds upon diffusion-based multi-view generation methods [26, 32], leveraging an image-conditioned diffusion model [42] as the core view generation backbone. By fine-tuning this model on synthetic human head data, we achieve two key advantages: (1) robust view consistency, enabled by strong priors from multi-view consistent training data, and (2) enhanced generalization capability, inherited from the large foundational model, ensuring accurate identity preservation during inference. In the second stage, we employ a state-of-the-art large reconstruction model [64] to fuse the generated sparse views into a comprehensive 3D Gaussian representation. Specifically, we fine-tune GS-LRM using synthetic human head data, enabling the reconstruction of detailed facial geometry and appearance.

We evaluate *FaceLift* both quantitatively and qualitatively across diverse datasets. Using real multi-view studio captures [34] and an independent synthetic human dataset [6], our approach consistently surpasses previous state-of-the-art methods across all evaluation metrics. Through extensive testing on in-the-wild portrait images,

we demonstrate that *FaceLift* reconstructs complete 3D heads with (1) fine-grained geometric and appearance details, (2) accurate identity preservation, and (3) high visual fidelity. Through comparisons with general object 3D reconstruction models and detailed ablation studies, we demonstrate that multi-view consistent training data plays a crucial role in achieving high-fidelity face reconstruction results.

Our contributions are summarized as follows:

- We propose *FaceLift*, a two-stage framework that reconstructs a high-fidelity 3D head from a single image using view generation and large reconstruction model.
- Our approach combines synthetic human head data for view-consistent training with the rich priors from a large image generation foundation model, enabling robust generalization capabilities.
- Through comprehensive quantitative and qualitative evaluation, we demonstrate that our approach achieves state-of-the-art performance in reconstruction accuracy and identity preservation.

## 2. Related Work

**Face Reconstruction.** 3D face reconstruction has long been a long-standing challenge in computer vision, with substantial progress driven by diverse approaches. Vetter and Blanz [54] pioneer a method for synthesizing 3D faces by linearly blending multiple 3D templates, now widely known as blendshapes. This work establishes the foundation for 3D Morphable Models (3DMMs), which represent 3D face shapes and textures as principal components derived from scanned data. Subsequent research [3, 4, 27, 29, 41] extend this framework, enabling the generation of new 3D faces by manipulating blending coefficients. However, these methods produce mesh-based representations that lack fine details and are limited to modeling the front of the face, excluding hair and 360-degree synthesis.

While 3DMM-based methods have been foundational, recent advances in deep learning, especially Generative Adversarial Networks (GANs) [15, 21, 22], have greatly improved 3D face synthesis quality. EG3D [62] uses a triplane NeRF representation with a pose-conditioned StyleGAN2 [22] framework. Follow-up works [2, 28] achieve single-image-to-3D generation through GAN inversion [7]. Despite their success, these methods can only synthesize near-frontal views. To overcome this, PanoHead [1] introduces a tri-grid neural volume representation, enabling full 360-degree head synthesis. Unfortunately, it does not provide a 3D head representation for consistent multi-view rendering. Recent efforts explore alternative representations for 3D face reconstruction from sparse input, such as a single image [13, 37, 55] or few-shot images [5]. However, these methods still require pre-instance optimization. Rodin [57] and its extension RodinHD [63] employ

an image-conditioned diffusion model to generate a triplane representation of a human head for full-head novel view synthesis. Nevertheless, their triplane diffusion model is limited to synthetic data and struggles to achieve high-fidelity reconstructions from real-world images.

**Synthetic Human Data.** Capturing high-quality 3D data of real humans requires a controlled studio environment and costly photography equipment [34]. As an alternative, large-scale synthetic 3D head datasets have emerged as an effective and resource-efficient solution for tasks like human head reconstruction [6, 57, 59, 63] and photorealistic relighting [61], offering a scalable way to train models without the restrictions of real-world data acquisition. Inspired by these previous works, we aim to use synthetic data to teach the model knowledge of the human head and minimize the generalization gap between synthetic data training and real-world inference.

**Image or Text to 3D.** Generative models have achieved remarkable success in 2D image generation with VAEs [24, 52], GANs [15, 21, 22], and diffusion models [19, 42, 48]. Building on this success, extensive research has extended these models to 3D content generation [14, 36, 38, 60]. Starting with DreamFusion [39], numerous works [31, 40, 45, 50, 58] try to distill NeRF [35, 62] or 3D Gaussians [23] representation from 2D image diffusion using a Score Distillation Sampling (SDS) loss. These methods can produce high-quality results but often encounter challenges such as slow optimization, over-saturated colors, and the Janus problem. To overcome these challenges, recent works [25, 26, 30, 32, 47] generate multi-view images with high consistency, which can be directly used for 3D reconstruction with neural reconstruction methods [23, 35, 56]. However, optimizing NeRF or NeuS remains far from real-time performance.

Recent advancements in large reconstruction models (LRMs) [20, 25, 51, 64] offer a pathway to faster 3D reconstruction. Leveraging scalable transformer architectures [11, 53] and large datasets like Objaverse [8, 9], these models effectively capture generalizable 3D priors. Unlike traditional pre-scene optimization methods [23, 35, 56], LRM employ a feed-forward approach, enabling the prediction of high-quality NeRF, mesh, or 3D Gaussian representations from sparse images in under a second. However, most of these research efforts are applied to general objects, with limited or suboptimal results demonstrating their ability on 3D head reconstruction.

### 3. Proposed Method

Given a single frontal image of a human face, our goal is to reconstruct a complete 3D head in the form of 3D Gaussian splats. We aim to generate plausible details not visible in the input view, such as the back of the head, while ensuring coherent visualization from any angle. Our proposed *FaceLift*

follows a two-stage pipeline, as shown in Fig 3. In the first stage, using multi-view synthetic images of human heads, we train an image-conditioned diffusion model to generate six views of a human head, maintaining multi-view consistency and preserving identity. These generated views, in the second stage, along with their corresponding camera poses, are then input into a fine-tuned GS-LRM model to reconstruct a set of 3D Gaussian splats.

#### 3.1. Synthetic Human Head Dataset

We implement a 3D head asset generation pipeline inspired by [59]. Our process begins with a collection of high-quality, artist-created 3D head meshes, which we enhance by incorporating detailed facial components, including eyes, teeth, gums, and both facial and scalp hair. We then augment these base models through rigging for pose variation and blendshape deformation for diverse facial expressions. The final head models are enriched with a set of PBR texture maps, including albedo, normal, roughness, specular, and subsurface scattering maps. At last, we dress the head model with a collection of clothing assets. The entire pipeline is implemented in Blender and the images are rendered with Cycles renderer.

To train our networks, we render images (samples shown in Fig. 4) at  $512 \times 512$  resolution from 200 unique identities, each with 50 varied appearances, including different hairstyles, skin tones, expressions, clothes, poses, etc. We render our training dataset under two types of lighting conditions: (1) ambient light and (2) random HDR environment light. We render six views for each subject to train the multi-view diffusion model. For fine-tuning GS-LRM [64], we render 32 views with random camera poses.

#### 3.2. Stage I: Single Image to Multi-view Generation

Recent 3D generation and reconstruction frameworks [25, 26, 32, 47] have demonstrated promising results by leveraging diffusion models to generate multi-view consistent images. Building on this approach, we adopt the open-source Stable Diffusion text-to-image generator [42] as the foundation of our view generation network. Specifically, we utilize the Stable Diffusion V2-1-unCLIP model [43], which is fine-tuned on Stable Diffusion V2-1 to incorporate CLIP image embeddings as additional conditioning input. In our pipeline, a CLIP image encoder processes the input frontal view face images, generating embeddings that serve as conditioning signals for the diffusion model.

To ensure the consistency of the generated novel views, we adopt a multi-view attention mechanism similar to [26, 32] to facilitate information propagation and implicitly encode multi-view dependencies. The diffusion model learns multi-view correlations by sharing information across views within the attention layers, allowing it to generate consistent RGB images from multiple perspectives.

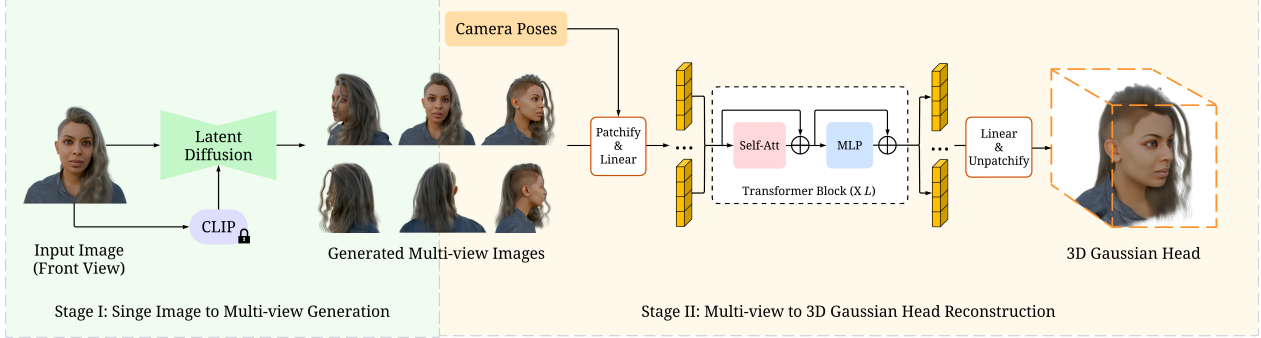


Figure 3. **Overview of FaceLift.** Given a single image of a human face as input, we train an image-conditioned, multi-view diffusion model to generate novel views covering the entire head. By leveraging pre-trained weights and high-quality synthetic data, our multi-view latent diffusion model can hallucinate unseen views of the human head with high-fidelity and multi-view consistency. We then fine-tune a GS-LRM [64], which takes multi-view images and their camera poses as input and generates 3D Gaussian splats to represent the human head. The generated 3D Gaussian representation enables full-head novel view synthesis.



Figure 4. **Synthetic data examples.** Top: six views for view generation. Bottom: samples of random views for GS-LRM training.

Given a single near frontal view face image with azimuth  $\alpha$ , the multi-view diffusion model will generate six views with azimuths equal to  $\{\alpha, \alpha \pm 45^\circ, \alpha \pm 90^\circ, \alpha + 180^\circ\}$ , covering 360 degrees of the human head. All images, both input and generated output, maintain a zero elevation angle, ensuring consistent horizontal viewpoints. The generated views consist of a reconstructed front view matching the input image, left and right profiles capturing the sides of the head, and a back view that synthesizes hair structure and color based on the frontal input and learned priors. We also generate three-quarter views (left-front and right-front) to enhance facial details in the following reconstruction stage.

### 3.3. Stage II: Multi-view to 3D Gaussian Head Reconstruction

Stage II conducts sparse view reconstruction using the six views generated by Stage I. For this task, we utilize GS-LRM [64], a state-of-the-art reconstruction model that excels at generating detailed 3D models from limited viewpoints. GS-LRM’s use of 3D Gaussians as its underlying representation is particularly effective for capturing the intricate details of human heads, such as hair strands. Furthermore, its feed-forward architecture enables rapid reconstruction, making it well-suited for practical applications.

GS-LRM employs a transformer architecture to regress pixel-aligned 3D Gaussians from a set of posed images. Each of the multi-view images is concatenated with its cor-

responding Plücker ray coordinates derived from the camera’s intrinsic and extrinsic parameters for pose conditioning. The images are divided into non-overlapping patches, with each 2D patch flattened into a 1D vector. A linear layer then maps these vectors to image patch tokens. The set of multi-view image tokens is concatenated and processed through a chain of transformer blocks. Later, the output tokens from the transformer are decoded into Gaussian parameters using a single linear layer. Then, the Gaussian parameters are unpatchified into Gaussians. Each 2D pixel corresponds to one 3D Gaussian. Gaussian is parameterized by 3-channel RGB, 3-channel scale, 4-channel rotation quaternion, 1-channel opacity, and 1-channel ray distance, similar to [23]. The final output of the GS-LRM model is the merge of 3D Gaussians from all input views.

During GS-LRM training, we randomly select four views from the available camera poses to reconstruct a total of eight views—four input views plus four novel viewpoints. Following [64], we optimize the model using a combination of MSE and perceptual losses. At inference time, GS-LRM processes the outputs from our multi-view diffusion model. While GS-LRM can accommodate any number of input views, we utilize all six views generated by the diffusion model to achieve optimal visual quality.

## 4. Experiments

To evaluate single-image head reconstruction methods, we leverage publicly available multiview head datasets to assess novel view synthesis performance using known camera parameters. We present both qualitative comparisons and quantitative error metrics across these datasets.

### 4.1. Experimental Setting

**Evaluation Datasets.** We evaluate our method using two multiview datasets: The synthetic Cafca dataset [6]: While this dataset shares our focus on faces, it differs significantly from our training dataset, which was independently devel-

oped. For evaluation, we select 40 subjects with 30 test camera poses each. Since the camera positions are randomly distributed, we manually select the most frontal view as input. The Ava-256 dataset [34]: This studio-captured dataset contains real human subjects. We sample 10 subjects and 10 test camera poses for our evaluation (more details are in the supplementary material). To demonstrate our system’s generalization capabilities, we also evaluate on a collected set of in-the-wild face images for qualitative assessment.

**Baselines.** We compare our results with three recent works: PanoHead [1], Era3D [26], and LGM [51]. PanoHead [1] is the state-of-the-art method for 3D full head reconstruction using 3D GANs. We perform GAN-inversion to obtain the reconstruction from a single input image. Note that it can only render images within a specific camera pose range and lacks a true 3D representation for novel view synthesis. Era3D [26] is a recent method for general object reconstruction. It employs a multi-view diffusion model to generate six views and uses the Instant-NSR-PL [17] implementation of NeuS [56] for mesh extraction. LGM [51], similar to GS-LRM [64], generates Gaussian splats as a 3D representation after a view generation stage.

**Evaluation Metric.** We evaluate reconstruction quality using four standard metrics: PSNR, SSIM, LPIPS [65], and DreamSim [12]. To evaluate identity preservation, we perform face verification using ArcFace [10] through the DeepFace [46] implementation.

**Implementation Details.** Both Cafca [6] and Ava-256 [34] datasets provide multi-view RGB images and corresponding camera poses. However, their camera systems differ from the ones utilized in *FaceLift* and baselines. We re-calculate the test camera extrinsic in each method’s camera system. For a more accurate comparison, we use the Mediapipe facial landmark detection algorithm [33] to identify facial landmarks in both target images and rendered outputs, aligning them based on landmark distributions. Details of this alignment process are provided in the supplementary material. Note that aligning images based on facial landmark detection only works for images that capture the front facial features.

## 4.2. Results on Cafca Dataset

We report numerical comparison results before and after facial landmark alignment in Tab. 1. Before facial landmark alignment, all 30 camera poses in the Cafca dataset are utilized as test views; some views do not cover the face region. Hence, we only report the face identity preservation metric ArcFace [10] in the aligned comparison. For the aligned comparison, each subject has 7 to 19 test views. The test views utilized in the experiment can be found in the supplementary material. In both comparisons, *FaceLift* performs favorably against baselines, especially for DreamSim [12],

Method	PSNR $\uparrow$	SSIM $\uparrow$	LPIPS $\downarrow$	DreamSim $\downarrow$	ArcFace $\downarrow$
PanoHead $^\dagger$ [1]	10.34	0.7282	0.3856	0.2507	—
Era3D $^\dagger$ [26]	11.41	0.6935	0.3884	0.3623	—
LGM $^\dagger$ [51]	12.41	0.7394	0.4013	0.2433	—
<i>FaceLift</i> $^\dagger$	<b>13.77</b>	<b>0.7514</b>	<b>0.3464</b>	<b>0.1678</b>	—
PanoHead [1]	10.72	0.7594	0.3351	0.2048	0.2183
Era3D [26]	13.69	0.7230	0.3662	0.2892	0.2978
LGM [51]	16.52	0.7933	0.3060	0.1552	0.2557
<i>FaceLift</i>	<b>16.61</b>	<b>0.7968</b>	<b>0.2694</b>	<b>0.1096</b>	<b>0.1573</b>

Table 1. **Numerical results on Cafca dataset [6].** We use  $\dagger$  to denote results obtained with images before facial landmark alignment. *FaceLift* achieves favorable performance on all evaluation metrics, especially for identity preservation metric ArcFace [10].



Figure 5. **Visual results on Cafca dataset [6].** *FaceLift* provides rendering results that closer align with the ground truth. Notice that PanoHead [1] can not handle the challenging hairstyle in row 1, Era3D [26] creates artifacts on the back of the head, and LGM [51] delivers inaccurate nose and jaw shapes.

which has a better alignment with human similarity judgments. It also achieves a better performance on identity preservation, demonstrated by a lower ArcFace [10] face embedding distance.

We show visual results on the Cafca dataset in Fig. 5. *FaceLift* renders novel views that better align with the ground truth, while other methods often fail to reconstruct the 3D head in correct colors or geometry structures.

## 4.3. Results on Ava-256 Dataset

We further evaluate *FaceLift* against other baselines on a studio-captured real human dataset, Ava-256 [44]. PanoHead [1] fails to produce reasonable results with the test camera poses in this dataset, so we exclude this baseline. Tab. 2 shows that *FaceLift* outperforms all other baselines across all evaluation metrics, demonstrating superior reconstruction quality and identity preservation. It also highlights *FaceLift*’s strong ability to generalize to real hu-

Method	PSNR $\uparrow$	SSIM $\uparrow$	LPIPS $\downarrow$	DreamSim $\downarrow$	ArcFace $\downarrow$
Era3D [26]	14.77	0.7963	0.2538	0.2515	0.3721
LGM [51]	14.05	0.8136	0.2476	0.1496	0.3142
<i>FaceLift</i>	<b>16.52</b>	<b>0.8271</b>	<b>0.2277</b>	<b>0.1065</b>	<b>0.1871</b>

Table 2. **Numerical results on Ava-256 dataset [44].** *FaceLift* performs favorably than baseline methods in both reconstruction metrics and identity facial identity metric, showing a better generalization ability towards real-captured human images.

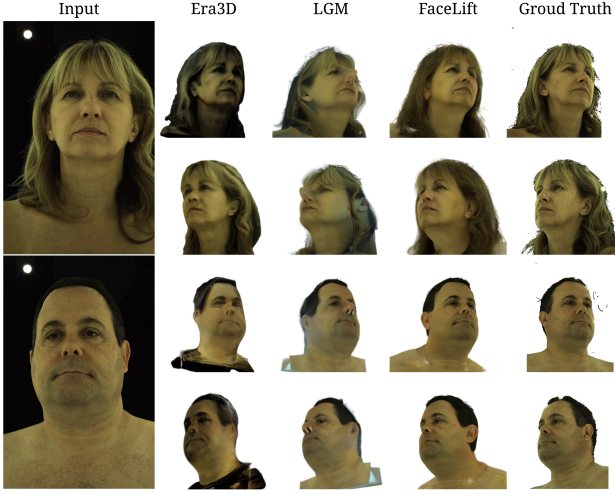


**Figure 6. Visual results on Ava-256 dataset [44].** Compared with baseline methods, *FaceLift* provides multi-view renderings that are more realistic and similar to ground truth. Era3D fails to deliver delicate facial structure, while LGM generates heads in inaccurate shapes and colors.

man faces. As shown in Fig. 6, *FaceLift* achieves more realistic head synthesis, while Era3D [26] struggles with accurate skin and hair textures, as well as facial details. LGM [51] produces inaccuracies in the nose shape.

#### 4.4. Results on In-the-wild Images

To further demonstrate *FaceLift*’s generalization ability and highlight its potential for real-world applications, we collect in-the-wild human face images and present qualitative results in comparison with other baselines in Fig. 7. Baseline methods often produce undesirable artifacts. For example, PanoHead [1] frequently fails to render the back of the head and occasionally generates extra eyes on the rear. It also struggles with accurately synthesizing hair, shadows, wrinkles, and facial paint. Meanwhile, PanoHead’s outputs lack multi-view consistency, as seen in the last row, where the girl continues to face the camera in novel view 1 despite a change in camera pose. Era3D [26] often struggles to produce an accurate head shape, particularly from the left and right views, and provides fewer geometric details compared to *FaceLift*. LGM [51] generates Gaussians with inaccurate color and opacity, and lacks a proper understanding of facial geometry, resulting in distorted facial features.

Moreover, we present more *FaceLift*’s novel view rendering results in Fig. 8 to demonstrate *FaceLift*’s ability to produce high-fidelity, realistic 3D head reconstructions with intricate details across a variety of challenging scenarios. *FaceLift* effectively handles faces under various lighting conditions. It can especially render realistic novel view

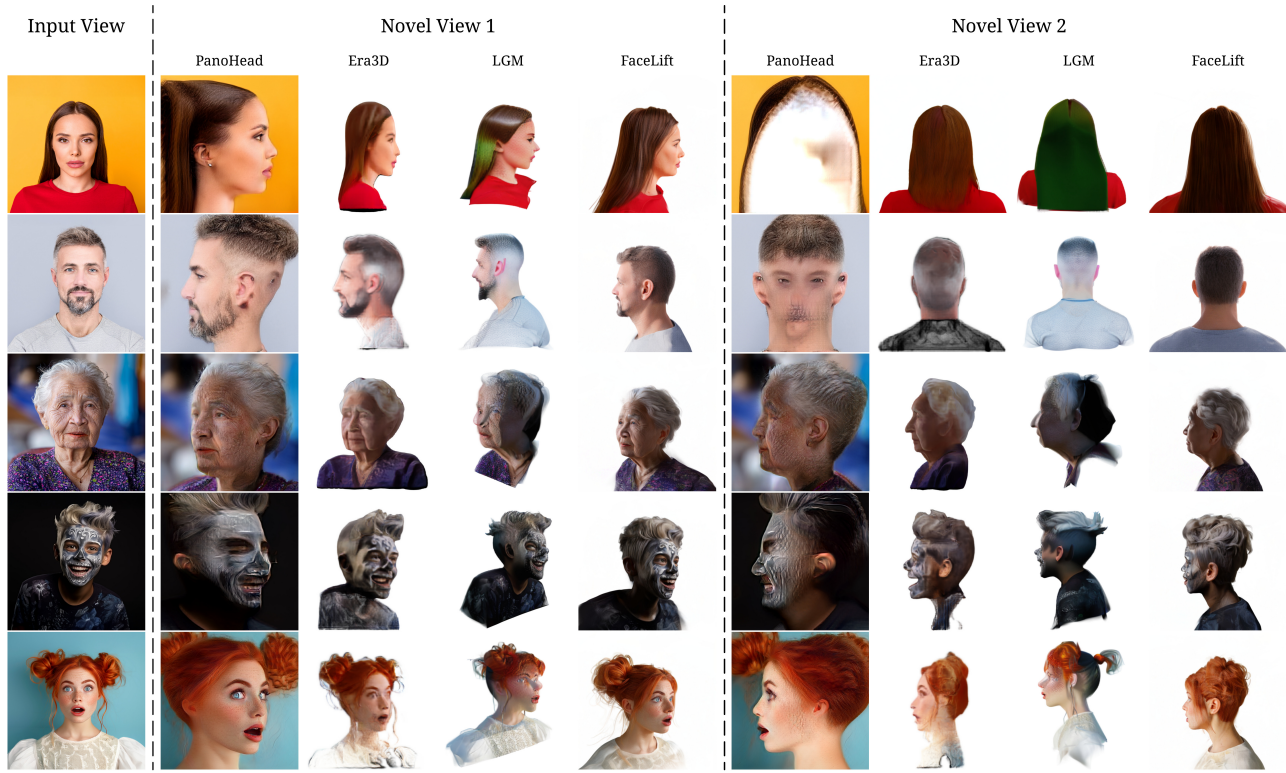


**Figure 7. Visual comparison on in-the-wild data.** *FaceLift* demonstrates great generalization ability and robustness towards in-the-wild images, provides realistic unseen view rendering results. Era3D [26] and LGM [51] generate 3D head representation in inaccurate shape. PanoHead [1] often creates severe artifacts on the back of the head and can not handle challenging hairstyles well.

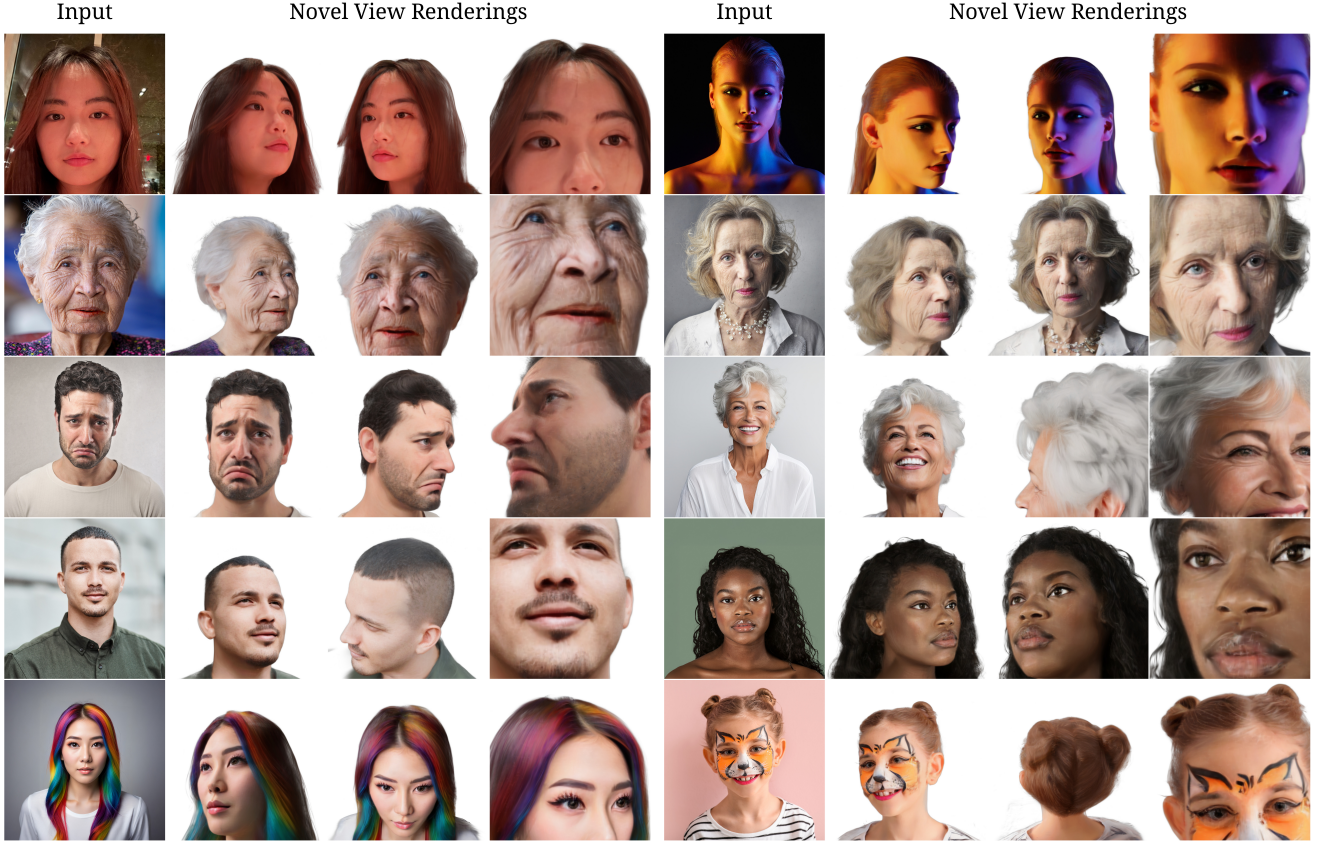


**Figure 8. Results of *FaceLift* on in-the-wild images.** *FaceLift* accurately reconstructs 3D head models under challenging lighting conditions, achieving high fidelity (row 1). It captures fine facial details such as wrinkles (row 2), mustaches, and individual hairs (row 3). Additionally, it remains robust to complex facial expressions (row 3), various skin tones (row 4), and hair colors (row 5). Furthermore, it can realistically reconstruct facial paint (row 5).

images given a photo captured with an iPhone under dark lighting conditions (row 1 column 1), emphasizing its robustness and potential for real-world application. It reconstructs facial details with high fidelity, especially the wrinkles and folds on the face caused by extreme expression (row 2, row 3). *FaceLift* also excels at reconstructing challenging textures, such as mustaches and hair. Furthermore, it faithfully reconstructs facial paint, despite such data not being included in our synthetic face dataset, showcasing its strong generalization ability.

#### 4.5. Application: Video as Input for 4D NVS

As shown in Fig. 9, benefits from the high-fidelity reconstruction ability, *FaceLift* can generate consistent 3D Gaussian sequence given a video as input to achieve 4D rendering. We process input video frames sequentially, generate one 3D Gaussian representation for each frame, and form a Gaussian sequence. Then, given any timestamp, we can select the corresponding 3D Gaussians from the Gaussian sequence and render from any given pose. Without any bells and whistles to constrain the consistency between differ-

ent timestamps, *FaceLift* can render video sequences under novel poses with minimal artifacts.

Combined with 2D face animation methods like LivePortrait [16], *FaceLift* achieves 3D face animation. Due to its robustness and strong generalizability, *FaceLift* can lift faces with extreme facial expressions to 3D without sacrificing fidelity. The results of this application are shown on our website.

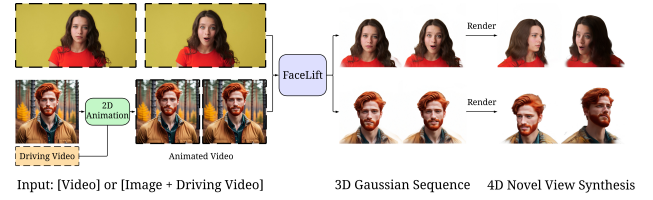


**Figure 9. Video as input for 4D rendering.** Given a video as input, *FaceLift* processes each frame sequentially and generates 3D Gaussian sequence. By rendering at a given camera pose and timestamp, *FaceLift* achieves 4D novel view synthesis.

## 4.6. Ablation Study

**Importance of Data with Diverse Lighting.** We use synthetic data to train our models, which offers the advantage of controlling lighting conditions and rendering head images under various lighting scenarios. In contrast, real-world human data is typically captured in a studio with lighting similar to ambient light, as shown in the input of Fig. 2. To highlight the importance of training models with diverse lighting conditions, we train *FaceLift* with (1) Data rendered with only ambient light, and (2) Data rendered in random HDR environment light. We present the visual result comparison in Fig. 10. The model trained exclusively on ambient light data struggles to understand shadows, often generating hair-like textures on the face. Furthermore, when exposed to strong light, it produces white regions on the face. In contrast, the model trained with random HDR environment light generates smooth transitions between regions with different lighting conditions.

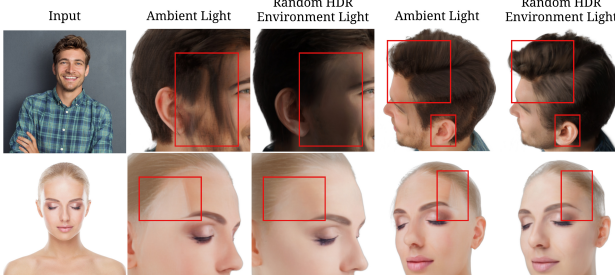


Figure 10. **Ablation study on synthetic data lighting condition.** Models trained only with ambient light struggle to handle shadows and strong lighting.

**Number Views for GS-LRM Reconstruction.** Vanilla GS-LRM [64] uses four views for inference. Instead, we add two more views, front-left and front-right, to further improve the reconstruction of the detailed facial structure. We compare baselines using different numbers of images as GS-LRM input in Fig. 11. With only four views, GS-LRM fails to reconstruct a complete forehead, while with six input views, GS-LRM can reconstruct eyes and eyebrows more smoothly. It also more realistically reconstructs challenging textures like wrinkles on the face and folds in the ears.

**Effectiveness of GS-LRM Fine-tuning.** GS-LRM [64] used in *FaceLift* is fine-tuned from the GS-LRM checkpoint pre-trained on Objaverse [8, 9] with synthetic human head data. To highlight the importance of training on synthetic human head data, we compare *FaceLift*'s rendering results with GS-LRM trained on Objaverse and our fine-tuned GS-LRM. Without fine-tuning, GS-LRM struggles to accurately estimate facial depth, resulting in artifacts around the eye region and a flat top of the head due to the ab-

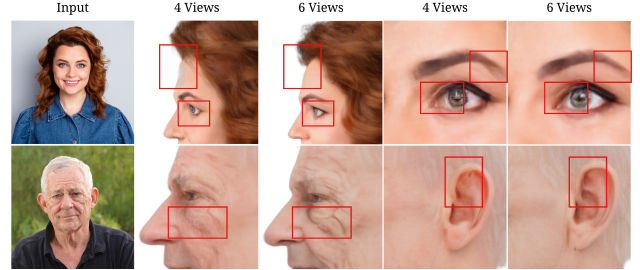


Figure 11. **Ablation study on number of input views to GS-LRM.** Using 6 views provides a more complete reconstruction of the forehead and delivers more accurate details on eyes and the geometry structure of wrinkles and ears.

sence of Gaussians splatted from above. After fine-tuning, the model learns prior knowledge of head structure, producing smoother and more realistic renderings.



Figure 12. **Ablation study on GS-LRM fine-tuning.** After fine-tuning, our GS-LRM reconstructor gains a more refined understanding of facial geometry, resulting in improved accuracy for facial features such as eyes, noses, and hair.

## 5. Conclusions and Future Work

We propose *FaceLift*, a feed-forward approach that lifts a single facial image to a detailed 3D reconstruction with preserved identity features. *FaceLift* uses multi-view diffusion to generate unobservable views and employs GS-LRM to reconstruct 3D Gaussian splats, enabling high-quality novel view synthesis. To overcome the difficulty of capturing real-world multi-view human head images, we render high-quality synthetic data for training and show that, despite being trained solely on synthetic data, *FaceLift* can reconstruct 3D heads from real-world captured images with high fidelity. Compared with baselines [1, 26, 51, 63], *FaceLift* generates 3D head representations with finer geometry and texture details and exhibits better identity preservation ability.

Furthermore, we demonstrate that *FaceLift* supports 4D novel view synthesis given a video sequence as input, demonstrating our method's high-fidelity results and robustness. Nevertheless, we still observe some inconsistencies across time stamps, especially with hair. To enhance temporal consistency, we plan to incorporate a 4D Gaussian representation in future work, allowing us to better constrain the position, shape, size, rotation, *etc.* of the 3D Gaussians across frames.

## 6. Acknowledgement

We appreciate the insightful discussions with Kai Zhang, Hao Tan, Zexiang Xu, Sai Bi, Sumit Chaturvedi, Hanwen Jiang, Yu-Ju Tsai, Kuan-Chih Huang, Chengxu Liu, and Dingyi Dai. We thank Nathan Carr and Kalyan Sunkavalli for their support.

## References

- [1] Sizhe An, Hongyi Xu, Yichun Shi, Guoxian Song, Umit Y Ogras, and Linjie Luo. Panohead: Geometry-aware 3d full-head synthesis in 360deg. In *CVPR*, 2023. [1](#), [2](#), [5](#), [6](#), [8](#)
- [2] Ananta R. Bhattacharai, Matthias Nießner, and Artem Sevestopolsky. Triplanenet: An encoder for eg3d inversion. In *WACV*, 2024. [2](#)
- [3] Volker Blanz and Thomas Vetter. A morphable model for the synthesis of 3d faces. In *Proceedings of the 26th Annual Conference on Computer Graphics and Interactive Techniques, SIGGRAPH*, 1999. [2](#)
- [4] James Booth, Anastasios Roussos, Stefanos Zafeiriou, Allan Ponniah, and David Dunaway. A 3d morphable model learnt from 10,000 faces. In *CVPR*, 2016. [2](#)
- [5] Marcel C Bühler, Kripasindhu Sarkar, Tanmay Shah, Gengyan Li, Daoye Wang, Leonhard Helminger, Sergio Orts-Escalano, Dmitry Lagun, Otmar Hilliges, Thabo Beeler, et al. Preface: A data-driven volumetric prior for few-shot ultra high-resolution face synthesis. In *ICCV*, 2023. [2](#)
- [6] Marcel C Bühler, Gengyan Li, Erroll Wood, Leonhard Helminger, Xu Chen, Tanmay Shah, Daoye Wang, Stephan Garbin, Sergio Orts-Escalano, Otmar Hilliges, et al. Cafca: High-quality novel view synthesis of expressive faces from casual few-shot captures. *arXiv preprint arXiv:2410.00630*, 2024. [2](#), [3](#), [4](#), [5](#), [12](#), [14](#)
- [7] Antonia Creswell and Anil Anthony Bharath. Inverting the generator of a generative adversarial network. In *TNNLS*. IEEE, 2018. [2](#)
- [8] Matt Deitke, Dustin Schwenk, Jordi Salvador, Luca Weihs, Oscar Michel, Eli VanderBilt, Ludwig Schmidt, Kiana Ehsani, Aniruddha Kembhavi, and Ali Farhadi. Objaverse: A universe of annotated 3d objects. In *CVPR*, 2023. [2](#), [3](#), [8](#)
- [9] Matt Deitke, Ruoshi Liu, Matthew Wallingford, Huong Ngo, Oscar Michel, Aditya Kusupati, Alan Fan, Christian Laforte, Vikram Voleti, Samir Yitzhak Gadre, et al. Objaverse-xl: A universe of 10m+ 3d objects. In *NeurIPS*, 2024. [2](#), [3](#), [8](#)
- [10] Jiankang Deng, Jia Guo, Jing Yang, Niannan Xue, Irene Kotaria, and Stefanos Zafeiriou. Arcface: Additive angular margin loss for deep face recognition. In *IEEE TPAMI*, 2022. [5](#)
- [11] Alexey Dosovitskiy. An image is worth 16x16 words: Transformers for image recognition at scale. *arXiv preprint arXiv:2010.11929*, 2020. [3](#)
- [12] Stephanie Fu, Netanel Tamir, Shobhita Sundaram, Lucy Chai, Richard Zhang, Tali Dekel, and Phillip Isola. Dreamsim: Learning new dimensions of human visual similarity using synthetic data. In *NeurIPS*, 2023. [5](#)
- [13] Chen Gao, Yichang Shih, Wei-Sheng Lai, Chia-Kai Liang, and Jia-Bin Huang. Portrait neural radiance fields from a single image. *arXiv preprint arXiv:2012.05903*, 2020. [2](#)
- [14] Jun Gao, Tianchang Shen, Zian Wang, Wenzheng Chen, Kangxue Yin, Dajiqing Li, Or Litany, Zan Gojcic, and Sanja Fidler. GET3D: A generative model of high quality 3d textured shapes learned from images. In *NeurIPS*, 2022. [3](#)
- [15] Ian Goodfellow, Jean Pouget-Abadie, Mehdi Mirza, Bing Xu, David Warde-Farley, Sherjil Ozair, Aaron Courville, and Yoshua Bengio. Generative adversarial nets. In *NeurIPS*, 2014. [1](#), [2](#), [3](#)
- [16] Jianzhu Guo, Dingyun Zhang, Xiaoqiang Liu, Zhizhou Zhong, Yuan Zhang, Pengfei Wan, and Di Zhang. Liveportrait: Efficient portrait animation with stitching and retargeting control. *arXiv preprint arXiv:2407.03168*, 2024. [7](#)
- [17] Yuan-Chen Guo. Instant neural surface reconstruction, 2022. <https://github.com/bennyguo/instant-nsr-pl>. [5](#)
- [18] Jonathan Ho and Tim Salimans. Classifier-free diffusion guidance. In *NeurIPS 2021 Workshop on Deep Generative Models and Downstream Applications*, 2021. [13](#)
- [19] Jonathan Ho, Ajay Jain, and Pieter Abbeel. Denoising diffusion probabilistic models. In *NeurIPS*, 2020. [1](#), [3](#)
- [20] Yicong Hong, Kai Zhang, Jiuxiang Gu, Sai Bi, Yang Zhou, Difan Liu, Feng Liu, Kalyan Sunkavalli, Trung Bui, and Hao Tan. LRM: large reconstruction model for single image to 3d. In *ICLR*, 2024. [3](#)
- [21] Tero Karras, Samuli Laine, and Timo Aila. A style-based generator architecture for generative adversarial networks. In *CVPR*, 2019. [2](#), [3](#)
- [22] Tero Karras, Samuli Laine, Miika Aittala, Janne Hellsten, Jaakko Lehtinen, and Timo Aila. Analyzing and improving the image quality of stylegan. In *CVPR*, 2020. [2](#), [3](#)
- [23] Bernhard Kerbl, Georgios Kopanas, Thomas Leimkühler, and George Drettakis. 3d gaussian splatting for real-time radiance field rendering. In *ACM TOG*, 2023. [1](#), [3](#), [4](#)
- [24] Diederik P. Kingma and Max Welling. Auto-encoding variational bayes. In *ICLR*, 2014. [3](#)
- [25] Jiahao Li, Hao Tan, Kai Zhang, Zexiang Xu, Fujun Luan, Yinghao Xu, Yicong Hong, Kalyan Sunkavalli, Greg Shakhnarovich, and Sai Bi. Instant3d: Fast text-to-3d with sparse-view generation and large reconstruction model. In *ICLR*, 2024. [2](#), [3](#)
- [26] Peng Li, Yuan Liu, Xiaoxiao Long, Feihu Zhang, Cheng Lin, Mengfei Li, Xingqun Qi, Shanghang Zhang, Wenhan Luo, Ping Tan, et al. Era3d: High-resolution multiview diffusion using efficient row-wise attention. *arXiv preprint arXiv:2405.11616*, 2024. [2](#), [3](#), [5](#), [6](#), [8](#)
- [27] Tianye Li, Timo Bolkart, Michael J Black, Hao Li, and Javier Romero. Learning a model of facial shape and expression from 4d scans. In *ACM TOG*, 2017. [1](#), [2](#)
- [28] Xuetong Li, Shalini De Mello, Sifei Liu, Koki Nagano, Umar Iqbal, and Jan Kautz. Generalizable one-shot 3d neural head avatar. In *NeurIPS*, 2024. [2](#)
- [29] Jiangke Lin, Yi Yuan, Tianjia Shao, and Kun Zhou. Towards high-fidelity 3d face reconstruction from in-the-wild images using graph convolutional networks. In *CVPR*, 2020. [2](#)

- [30] Minghua Liu, Chao Xu, Haian Jin, Linghao Chen, Mukund Varma T., Zexiang Xu, and Hao Su. One-2-3-45: Any single image to 3d mesh in 45 seconds without per-shape optimization. In *NeurIPS*, 2023. 3
- [31] Ruoshi Liu, Rundi Wu, Basile Van Hoorick, Pavel Tokmakov, Sergey Zakharov, and Carl Vondrick. Zero-1-to-3: Zero-shot one image to 3d object. In *ICCV*, 2023. 2, 3
- [32] Xiaoxiao Long, Yuan-Chen Guo, Cheng Lin, Yuan Liu, Zhiyang Dou, Lingjie Liu, Yuexin Ma, Song-Hai Zhang, Marc Habermann, Christian Theobalt, et al. Wonder3d: Single image to 3d using cross-domain diffusion. In *CVPR*, 2024. 2, 3
- [33] Camillo Lugaressi, Jiuqiang Tang, Hadon Nash, Chris Mc-Clanahan, Esha Uboweja, Michael Hays, Fan Zhang, Chuo-Ling Chang, Ming Guang Yong, Juhyun Lee, et al. Mediapipe: A framework for building perception pipelines. *arXiv preprint arXiv:1906.08172*, 2019. 5
- [34] Julieta Martinez, Emily Kim, Javier Romero, Timur Bagautdinov, Shunsuke Saito, Shou-I Yu, Stuart Anderson, Michael Zollhöfer, Te-Li Wang, Shaojie Bai, Chenghui Li, Shih-En Wei, Rohan Joshi, Wyatt Borsos, Tomas Simon, Jason Saragih, Paul Theodosis, Alexander Greene, Anjani Josyula, Silvio Mano Maeta, Andrew I. Jewett, Simon Venstain, Christopher Heilman, Yueh-Tung Chen, Sidi Fu, Mohamed Ezzeldin A. Elshaer, Tingfang Du, Longhua Wu, Shen-Chi Chen, Kai Kang, Michael Wu, Youssef Emad, Steven Longay, Ashley Brewer, Hitesh Shah, James Booth, Taylor Koska, Kayla Haidle, Matt Andromalos, Joanna Hsu, Thomas Dauer, Peter Selednik, Tim Godisart, Scott Ardisson, Matthew Cipperly, Ben Humberston, Lon Farr, Bob Hansen, Peihong Guo, Dave Braun, Steven Krenn, He Wen, Lucas Evans, Natalia Fadeeva, Matthew Stewart, Gabriel Schwartz, Divam Gupta, Gyeongsik Moon, Kaiwen Guo, Yuan Dong, Yichen Xu, Takaaki Shiratori, Fabian Prada, Bernardo R. Pires, Bo Peng, Julia Buffalini, Autumn Trimble, Kevyn McPhail, Melissa Schoeller, and Yaser Sheikh. Codec Avatar Studio: Paired Human Captures for Complete, Driveable, and Generalizable Avatars. In *NeurIPS*, 2024. 2, 3, 5, 12, 14, 15
- [35] Ben Mildenhall, Pratul P. Srinivasan, Matthew Tancik, Jonathan T. Barron, Ravi Ramamoorthi, and Ren Ng. Nerf: Representing scenes as neural radiance fields for view synthesis. In  *ECCV*, 2020. 1, 3
- [36] Roy Or-El, Xuan Luo, Mengyi Shan, Eli Shechtman, Jeong Joon Park, and Ira Kemelmacher-Shlizerman. Stylesdf: High-resolution 3d-consistent image and geometry generation. In *CVPR*, 2022. 3
- [37] Foivos Paraperas Papantoniou, Alexandros Lattas, Stylianos Moschoglou, and Stefanos Zafeiriou. Relightify: Relightable 3d faces from a single image via diffusion models. In *ICCV*, 2023. 2
- [38] Dario Pavllo, Graham Spinks, Thomas Hofmann, Marie-Francine Moens, and Aurélien Lucchi. Convolutional generation of textured 3d meshes. In *NeurIPS*, 2020. 3
- [39] Ben Poole, Ajay Jain, Jonathan T. Barron, and Ben Mildenhall. Dreamfusion: Text-to-3d using 2d diffusion. In *ICLR*, 2023. 3
- [40] Guocheng Qian, Jinjie Mai, Abdullah Hamdi, Jian Ren, Aliaksandr Siarohin, Bing Li, Hsin-Ying Lee, Ivan Skorokhodov, Peter Wonka, Sergey Tulyakov, et al. Magic123: One image to high-quality 3d object generation using both 2d and 3d diffusion priors. *arXiv preprint arXiv:2306.17843*, 2023. 3
- [41] Elad Richardson, Matan Sela, and Ron Kimmel. 3d face reconstruction by learning from synthetic data. In *International Conference on 3D Vision*, 2016. 2
- [42] Robin Rombach, Andreas Blattmann, Dominik Lorenz, Patrick Esser, and Björn Ommer. High-resolution image synthesis with latent diffusion models. In *CVPR*, 2022. 2, 3
- [43] Robin Rombach, Andreas Blattmann, Dominik Lorenz, Patrick Esser, and Björn Ommer. High-resolution image synthesis with latent diffusion models. In *CVPR*, 2022. 3, 13
- [44] Shunsuke Saito, Gabriel Schwartz, Tomas Simon, Junxuan Li, and Giljoo Nam. Relightable gaussian codec avatars. In *CVPR*, 2024. 5, 6
- [45] Kyle Sargent, Zizhang Li, Tanmay Shah, Charles Herrmann, Hong-Xing Yu, Yunzhi Zhang, Eric Ryan Chan, Dmitry Lagun, Li Fei-Fei, Deqing Sun, et al. Zeronvs: Zero-shot 360-degree view synthesis from a single real image. In *CVPR*, 2024. 3
- [46] Sefik Ilkin Serengil and Alper Ozpinar. Hyperextended light-face: A facial attribute analysis framework. In *ICEET*, 2021. 5
- [47] Ruoxi Shi, Hansheng Chen, Zhuoyang Zhang, Minghua Liu, Chao Xu, Xinyue Wei, Linghao Chen, Chong Zeng, and Hao Su. Zero123++: a single image to consistent multi-view diffusion base model, 2023. 2, 3
- [48] Jiaming Song, Chenlin Meng, and Stefano Ermon. Denoising diffusion implicit models. In *ICLR*, 2021. 3, 13
- [49] Wenqiang Sun, Shuo Chen, Fangfu Liu, Zilong Chen, Yueqi Duan, Jun Zhang, and Yikai Wang. Dimensionx: Create any 3d and 4d scenes from a single image with controllable video diffusion, 2024. 12
- [50] Jiaxiang Tang, Jiawei Ren, Hang Zhou, Ziwei Liu, and Gang Zeng. Dreamgaussian: Generative gaussian splatting for efficient 3d content creation. *arXiv preprint arXiv:2309.16653*, 2023. 3
- [51] Jiaxiang Tang, Zhaoxi Chen, Xiaokang Chen, Tengfei Wang, Gang Zeng, and Ziwei Liu. Lgm: Large multi-view gaussian model for high-resolution 3d content creation. *arXiv preprint arXiv:2402.05054*, 2024. 3, 5, 6, 8
- [52] Aäron van den Oord, Oriol Vinyals, and Koray Kavukcuoglu. Neural discrete representation learning. In *NeurIPS*, 2017. 3
- [53] Ashish Vaswani, Noam Shazeer, Niki Parmar, Jakob Uszkoreit, Llion Jones, Aidan N. Gomez, Łukasz Kaiser, and Illia Polosukhin. Attention is all you need. In *NeurIPS*, 2017. 3
- [54] Thomas Vetter and Volker Blanz. Estimating coloured 3d face models from single images: An example based approach. In *ECCV*, 1998. 1, 2
- [55] Vishal Vinod, Tanmay Shah, and Dmitry Lagun. Teglo: High fidelity canonical texture mapping from single-view images. In *WACV*, 2024. 2

- [56] Peng Wang, Lingjie Liu, Yuan Liu, Christian Theobalt, Taku Komura, and Wenping Wang. Neus: Learning neural implicit surfaces by volume rendering for multi-view reconstruction. In *NeurIPS*, 2021. [3](#), [5](#)
- [57] Tengfei Wang, Bo Zhang, Ting Zhang, Shuyang Gu, Jianmin Bao, Tadas Baltrusaitis, Jingjing Shen, Dong Chen, Fang Wen, Qifeng Chen, et al. Rodin: A generative model for sculpting 3d digital avatars using diffusion. In *CVPR*, 2023. [2](#), [3](#)
- [58] Zhengyi Wang, Cheng Lu, Yikai Wang, Fan Bao, Chongxuan Li, Hang Su, and Jun Zhu. Prolificdreamer: High-fidelity and diverse text-to-3d generation with variational score distillation. In *NeurIPS*, 2024. [3](#)
- [59] Erroll Wood, Tadas Baltrušaitis, Charlie Hewitt, Sebastian Dziadzio, Thomas J Cashman, and Jamie Shotton. Fake it till you make it: face analysis in the wild using synthetic data alone. In *ICCV*, 2021. [3](#)
- [60] Jiajun Wu, Chengkai Zhang, Tianfan Xue, Bill Freeman, and Josh Tenenbaum. Learning a probabilistic latent space of object shapes via 3d generative-adversarial modeling. In *NeurIPS*, 2016. [3](#)
- [61] Yu-Ying Yeh, Koki Nagano, Sameh Khamis, Jan Kautz, Ming-Yu Liu, and Ting-Chun Wang. Learning to relight portrait images via a virtual light stage and synthetic-to-real adaptation. In *ACM TOG*, 2022. [3](#)
- [62] Ziyang Yuan, Yiming Zhu, Yu Li, Hongyu Liu, and Chun Yuan. Make encoder great again in 3d gan inversion through geometry and occlusion-aware encoding. In *ICCV*, 2023. [1](#), [2](#), [3](#)
- [63] Bowen Zhang, Yiji Cheng, Chunyu Wang, Ting Zhang, Jiaolong Yang, Yansong Tang, Feng Zhao, Dong Chen, and Baineng Guo. Rodinhd: High-fidelity 3d avatar generation with diffusion models. In *ECCV*, 2024. [1](#), [2](#), [3](#), [8](#)
- [64] Kai Zhang, Sai Bi, Hao Tan, Yuanbo Xiangli, Nanxuan Zhao, Kalyan Sunkavalli, and Zexiang Xu. Gs-lrm: Large reconstruction model for 3d gaussian splatting. In *ECCV*, 2024. [2](#), [3](#), [4](#), [5](#), [8](#), [13](#)
- [65] Richard Zhang, Phillip Isola, Alexei A. Efros, Eli Shechtman, and Oliver Wang. The unreasonable effectiveness of deep features as a perceptual metric. In *CVPR*, 2018. [5](#)

# FaceLift: Single Image to 3D Head with View Generation and GS-LRM

## Supplementary Material

### A. Overview

This supplementary material presents additional results to complement the main manuscript. We provide further experiments in Sec. B, including a comparison with DimensionX [49] and additional visual results of *FaceLift* on in-the-wild images. We illustrate experimental details in Sec. C. Finally, we discuss the limitations of *FaceLift* in Sec. D.

### B. Additional Experiments

#### B.1. Comparison with DimensionX

We provide comparison results on single image to 3D tasks with a state-of-the-art video diffusion model, DimensionX [49]. DimensionX is a framework designed to generate photorealistic 3D and 4D scenes from a single image with video diffusion. The results are shown in Fig. 13. As a video diffusion model, DimensionX struggles to produce multi-view consistent results and lacks a clear spatial understanding of head shapes. As a result, it often generates eyes gazing in the wrong direction and ears positioned incorrectly, along with inaccurate shoulder shapes. In contrast, *FaceLift* generates highly realistic 3D human heads while also producing more visually striking hair.

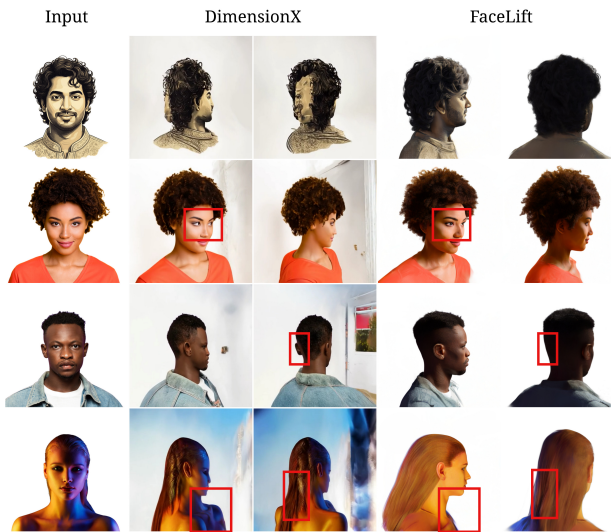


Figure 13. **Visual comparison with DimensionX.** DimensionX frequently produces inaccuracies in the back of the head and the shoulder shapes. Other common issues include misaligned ears and eyes gazing in incorrect directions. Additionally, controlling camera poses is challenging. In contrast, *FaceLift* delivers results that are significantly more consistent across multiple views while enabling the generation of more visually appealing hair.

### B.2. Additional Results on In-the-wild Images

We present additional results on in-the-wild images in Fig. 14. *FaceLift* demonstrates the ability to effectively handle diverse hairstyles and beards. Notably, it excels at hallucinating unobservable hairline splits and synthesizing the transparent properties of hair using Gaussians with low opacity. *FaceLift* reconstructs photo-realistic 3D heads under various lighting conditions and can be further extended to the reconstruction of cartoon characters.

### C. Experimental Details

#### C.1. Details on Benchmark Evaluation

**Test Camera Extrinsic.** Both the Cafca [6] and Ava256 [34] datasets offer multi-view RGB images along with corresponding camera poses. However, their camera systems differ from those used in *FaceLift* and the baselines. Directly applying their camera poses for inference is infeasible. Hence, we recalculate the test camera extrinsic in each method’s camera system with the following procedure.

The Ava-256 dataset uses a world coordinate system with the origin set at one of the camera positions. We first re-center the world coordinate origin to the midpoint of all camera locations, which is approximately the center of the human head. This step is unnecessary for the Cafca dataset, as its world coordinate origin is defined as the head’s center. Next, we compute the rotation transformation from the test camera pose to the input camera pose within the dataset’s coordinate system. We then apply the same transformation to the input camera pose in each method’s camera system and rescale the translation to match the settings of each method to get the test camera extrinsic under each method’s camera system. After applying the camera pose transformation, perfect alignment is not achieved due to differences in camera distance and intrinsic parameters. To address this, we manually crop and scale the rendered images for closer alignment with the target images.

**Facial Landmark Alignment.** To align two images based on their facial landmarks, we first compute the geometric transformations—scale and translation—that align the landmarks of one image with the landmarks of the other. Given an input image  $I_1$  and two sets of corresponding facial landmarks  $L_1$  and  $L_2$ , we begin by calculating the centroids of the landmark sets, centering the landmarks around their respective centroids. Next, we compute the uniform scaling factor and translation vector that minimize the difference between the centered landmarks. These transformations are then applied to the input image  $I_1$ , producing the trans-



Figure 14. **Results of FaceLift on in-the-wild images.** FaceLift is capable of reconstructing complex facial hair, including a variety of hairstyles and beards. It can also accurately handle dramatic facial expressions and varying lighting conditions. Additionally, it is well-suited for the reconstruction of cartoon characters.

formed image  $I_t$  in which the facial landmarks are aligned with those of  $L_2$ . This process is illustrated in Algorithm 1.

## C.2. Implementation Details

**Multi-view Diffusion.** Our multi-view diffusion model is built based on the open-source latent diffusion framework, Stable Diffusion V2-1-unCLIP model [43]. The model is trained on eight A100 GPUs (each with 80 GB of memory) using a batch size of 64 over 20,000 steps, with a learning rate of 1e-4. For classifier-free guidance (CFG) [18], the CLIP condition was randomly omitted at a rate of 0.05 during training. During inference, we utilized the DDIM

sampler [48] with 50 steps and a guidance scale of 3.0 to generate multi-view images. Both the input and output images have a resolution of  $512 \times 512$ .

**GS-LRM.** For fine-tuning GS-LRM, we mostly maintain the original setup described in [64]. During each training step, we randomly sample a set of 8 images (4 as input views and 4 as supervision views) from 32 random HDR environment light renderings. Both input and output images are rendered at a resolution of  $512 \times 512$ . The model is fine-tuned for 20,000 steps using eight A100 GPUs, each equipped with 40 GB of memory.

---

**Algorithm 1:** Image Alignment via Facial Landmarks

---

```

Input: Image  $I_1$ , Landmarks  $L_1, L_2$ 
Output: Transformed image  $I_t$ 

1 Function
    GetTransformFromLandmarks( $L_1, L_2$ ):
2     Compute centroids  $C_1, C_2$  of  $L_1, L_2$ ;
3     Center landmarks:  $L'_1 \leftarrow L_1 - C_1$ ,
         $L'_2 \leftarrow L_2 - C_2$ ;
4     Compute scale:  $s \leftarrow \frac{\sum(L'_1 \cdot L'_2)}{\sum(L'_1 \cdot L'_1)}$ ;
5     Compute translation:  $t \leftarrow C_2 - s \cdot C_1$ ;
6     return  $s, t$ ;
7 Function ApplyTransformToImage( $I, s, t$ ):
8     Create transformation matrix  $M$ ;
9     Transform image:  $I_t \leftarrow \text{warpAffine}(I, M)$ ;
10    return  $I_t$ ;
11 Function
    TransformImageWithLandmarks( $I_1, L_1, L_2$ ):
12    Compute  $s, t \leftarrow$ 
        GetTransformFromLandmarks( $L_1, L_2$ );
13    Transform image:
         $I_t \leftarrow \text{ApplyTransformToImage}(I_1, s, t)$ ;
14    return  $I_t$ ;

```

---

### C.3. Datasets

**Cafca Dataset.** The Cafca dataset [6] comprises 1,500 identities, 30 camera poses, 13 expressions, and three environments. From this, we select 40 identities, as detailed in Tab. 3. We utilize the first expression and the first environment (folder 00000\_000) for each identity. The input view corresponding to each identity is also specified in Tab. 3. In experiments without facial landmark alignment, all 30 camera poses are used. For experiments with facial landmark alignment, the test views employed are outlined in Tab. 3.

**Ava-256 Dataset.** The Ava-256 dataset [34] consists of 256 identities, each captured by 80 cameras, with over 5,000 frames per camera. For qualitative evaluation, we select 10 identities, each with 10 test camera views. All selected frames feature natural expressions. We use camera 401168 as the input view, as it captures the front view of the faces and is positioned at the center of Ava-256’s world coordinate system. The input view, test views, and corresponding frame IDs are detailed in Tab. 4.

### D. Limitations

*FaceLift* achieves high-fidelity, photorealistic 3D head reconstruction from a single input image. It provides detailed representations of hair and skin texture while demonstrating superior identity preservation compared to existing meth-

ID	Input View	Test Views
00000	26	00 02 06 08 10 11 12 13 17 19 20 23 24 26
00002	12	00 03 04 05 06 07 08 09 12 13 15 17 21 22 23 24 25
00004	07	03 04 07 09 10 11 18 19 23 24 25 26 27 29
00005	15	01 02 06 07 08 10 11 13 15 18 19 20 21 23 26 27 28
00006	27	00 02 10 19 20 23 27
00007	09	03 04 09 11 13 15 16 17 19 21 24 26 28
00010	24	02 04 08 10 12 13 14 15 17 21 22 23 24 25 26 27 28 29
00011	07	02 05 07 09 11 12 14 16 24 27 29
00014	03	02 03 06 12 14 17 22 23 25 28 29
00015	22	00 02 04 06 09 12 14 15 20 22 24 27 28
00017	12	01 02 07 12 14 15 16 17 20 22 23 24 25 26
00018	08	00 02 06 08 09 13 16 18 20 25 26
00019	14	00 04 05 06 10 12 13 14 16 17 18 20 21 22 26 28
00020	01	00 01 03 04 06 07 10 14 16 17 19 22 23 25 26 27 29
00021	11	02 03 05 07 08 09 11 14 15 17 19 21 22 23 26
00022	18	00 01 03 07 08 09 11 12 17 18 19 21 22 24 26 28
00023	03	00 03 05 06 08 12 14 18 24 25 27
00028	18	04 05 06 10 12 13 16 18 19 22 24 25 28 29
00030	21	00 01 02 03 06 07 08 11 14 17 19 21 22 24 26
00033	03	00 03 06 11 12 13 15 19 21 22 24 27 28
00034	10	01 06 07 09 10 13 15 16 17 18 19 23 25 28
00048	04	00 01 02 04 05 06 07 10 12 15 20 23 24 25 27 28
00051	26	03 07 10 11 15 17 19 21 22 24 26 28 29
00056	07	00 01 02 07 08 12 14 15 17 18 20 21 22 23 24 25 28 29
00057	11	00 01 02 03 05 06 08 11 12 14 17 18 19 22 26 29
00063	01	01 02 05 08 09 11 13 14 16 17 18 20 22 25 26 28 29
00066	13	01 05 06 07 12 13 21 22 26 27
00068	12	00 01 06 10 12 14 16 19 21 22 25 26 27
00072	25	02 04 05 10 12 13 14 17 25 26
00078	20	00 02 03 05 06 07 08 12 13 14 15 16 17 18 20 24 25 28 29
00080	08	01 03 04 05 06 08 10 12 14 15 16 17 22 24 26 27
00082	16	05 06 07 09 13 16 17 19 20 23 25 27
00083	16	00 02 03 04 05 08 09 13 14 16 17 19 21 22 24 25 27 29
00084	01	02 04 08 09 11 12 14 16 17 18 19 23 28 29
00086	13	00 01 03 04 08 09 13 14 17 18 19 20 22 23 24
00087	01	00 01 02 04 07 08 09 12 15 16 17 18 21 24 26 27
00094	08	02 05 08 09 12 19 24 25 27
00095	08	00 01 03 04 08 09 10 11 13 14 18 19 20 21 24 28 29
00096	01	01 05 07 10 12 17 19 21 22 28
00099	00	00 02 03 04 05 07 08 09 12 14 15 16 17 20 21 23 25 29

Table 3. **Identities and views used for the experiment on Cafca dataset [6].**

ods.

Despite these appealing results, our approach has certain limitations. First, our synthetic dataset does not include accessories such as hats or glasses. As a result, when the input

ID	Frame ID	Input View	Test Views
20210810–1306–FXN596	029693	401168	400944 400981 401031 401075 401163 401175 401292 401303 401316 401463
20210827–0906–KDA058	028930	401168	400944 401031 401071 401163 401166 401292 401316 401408 401410 401458
20210901–0833–LAS440	027655	401168	400944 401031 401161 401163 401172 401292 401303 401316 401410 401458
20210929–0827–MCR809	029457	401168	400981 401070 401158 401166 401173 401305 401313 401408 401410 401458
20211001–0855–KJJ701	032309	401168	400939 401031 401163 401166 401292 401316 401408 401410 401452 401458
20220215–0801–ONK705	027201	401168	400944 401031 401045 401163 401166 401172 401408 401410 401463 401469
20220310–1128–ZSC414	028601	401168	400942 401031 401045 401163 401164 401166 401303 401408 401410 401411
20220712–1040–JEH262	030060	401168	400944 400981 401031 401045 401163 401408 401410 401452 401458 401469
20220809–1321–UTC375	027432	401168	401031 401071 401163 401166 401175 401292 401303 401452 401458 401469
20220818–1653–SSF476	036588	401168	400981 401031 401071 401163 401166 401175 401408 401410 401458 401469

Table 4. Identities and views used for the experiments on Avav256 dataset [34].



Figure 15. Limitation of *FaceLift*. Due to the absence of accessories in the training data, our method often generates hair-like textures to approximate hats. Additionally, it occasionally produces extraneous hair when encountering out-of-distribution images.

image features a hat, the model may generate hair-like textures to approximate the back of the hat, as illustrated in Fig. 15, row 1. This limitation could be addressed by incorporating synthetic data with accessories. Additionally, when handling out-of-distribution inputs, such as those in Fig. 15, row 2, the model occasionally generates extraneous hair. This issue might be mitigated by refining the training data distribution or introducing text prompts to enhance control over the multi-view diffusion generation process.